Monthly Notices of the ROYAL ASTRONOMICAL SOCIETY
MNRAS **463,** 3398–3408 (2016) doi:10.1093/mnras/stw2234

# On the deceleration of relativistic jets in active galactic nuclei – I. Radiation drag

V. S. Beskin[1,2]★ and A. V. Chernoglazov[2]

[1]*Lebedev Physical Institute, Russian Academy of Sciences, Leninsky prospekt 53, Moscow 119991, Russia*
[2]*Moscow Institute of Physics and Technology, Institutsky per. 9, Dolgoprudny 141700, Russia*

Accepted 2016 September 1. Received 2016 September 1; in original form 2016 June 20

**ABSTRACT**

Deceleration of relativistic jets from active galactic nuclei (AGNs) detected recently by the Monitoring Of Jets in Active galactic nuclei with Very Long Baseline Array Experiments (MOJAVE) team is discussed in connection with the interaction of the jet material with an external photon field. The appropriate energy density of the isotropic photon field necessary to decelerate jets is determined. It is shown that disturbances of the electric potential and magnetic surfaces play an important role in the general dynamics of particle deceleration.

**Key words:** radiation mechanisms: non-thermal – galaxies: active – galaxies: jets – quasars: general – radio continuum: galaxies.

## 1 INTRODUCTION

Recent progress in Very Long Baseline Interferometry (VLBI) observations of relativistic jets outflowing from active galactic nuclei (Lobanov 1998; Cohen et al. 2007; Clausen-Brown et al. 2013; Kardashev et al. 2014) gives us new information concerning their physical characteristics and dynamics. In particular, a rather effective deceleration of the jet material on scales greater than 50–100 pc was recently detected by the Monitoring Of Jets in Active galactic nuclei with Very Long Baseline Array Experiments (MOJAVE) team (Homan et al. 2015). We will consider one possible explanation for such deceleration, connected to the interaction of the jet with the external photon field. Both radiation drag and particle loading will be considered in detail in terms of the standard magnetohydrodynamics (MHD) approach, the first mechanism below and the second one in the accompanying article (Beskin & Nokhrina in preparation).

Note that the frame for our work is the MHD model, now developed intensively in connection with the theory of relativistic jets outflowing from rotating supermassive ($M \sim 10^8$–$10^9\,\mathrm{M}_\odot$) black holes, which are thought of as the 'central engine' in active galactic nuclei and quasars (Begelman, Blandford & Rees 1984; Thorne, Price & Macdonald 1986). In particular, the MHD model is the most popular theory of jet origin and stability. Moreover, for the last few years, additional observational confirmation in favour of the MHD model, such as the presence of $e^+e^-$ plasma (Reynolds et al. 1996; Hirotani & Okamoto 1998) and also a toroidal magnetic field (Gabuzda, Murrey & Cronin 2005), has been found. Finally, recent numerical simulations (Komissarov et al. 2007; Porth et al. 2011; McKinney, Tchekhovskoy & Blanford 2012) demonstrate very nice agreement with MHD analytical asymptotic solutions.

On the other hand, the density of photons in the vicinity of the central engine is high enough that it may lead to a situation in which the photon field dramatically changes the characteristics of the ideal MHD outflow. These changes may result in particle loading, i.e. extensive $e^+e^-$ pair creation (Svensson 1984), acceleration through the action of the radiation drag force for small enough particle energy and also deceleration of highly energetic particles (Sikora et al. 1996). In other words, for a self-consistent consideration to be achieved, the interaction of a magnetically dominated flow with an external photon field should be taken into account.

Unfortunately, for many years the study of these two processes, i.e. MHD acceleration and the action of external photons, has developed separately. Only in the article by Li, Begelman & Chiueh (1992) was the first analytical step taken to combine them. In particular, the authors demonstrated how general equations can be integrated for conical geometry (which is impossible in the general case). On the other hand, these results were obtained in the given (exactly monopolar) poloidal magnetic field. However, under this assumption the fast magnetosonic surface (for cold flow) is located at infinity (Michel 1969; Kennel, Fujimura & Okamoto 1976; Lery et al. 1998). As a result, it is impossible to analyse the radiation drag effect in the vicinity of the fast magnetosonic surface and the properties of the supersonic flow outside this surface.

A self-consistent disturbance of magnetic surfaces was analysed by Beskin, Zakamska & Sol (2004) for high enough particle energy (the situation in which the radiation pressure is ineffective in particle acceleration). It was demonstrated that, in the case of magnetically dominated flow, the drag force does not actually change the particle energy and only diminishes the total energy flux. It was shown that the disturbance of magnetic surfaces becomes large only if the drag force changes the total energy flux significantly. Finally, Russo &

★ E-mail: beskin@lpi.ru

© 2016 The Authors
Published by Oxford University Press on behalf of the Royal Astronomical Society

Downloaded from http://mnras.oxfordjournals.org/ by guest on October 10, 2016

Thompson (2013a,b) have recently considered the drag action on a magnetized outflow in gamma-bursters, where radiation pressure can play the leading role in particle acceleration.

Regarding particle loading, several aspects of this process were considered by Svensson (1984), Lyutikov (2003), Derishev et al. (2003) and Stern & Poutanen (2006). Even if electron–positron pairs are created at rest (and hence do not change the total energy and angular momentum flux), increasing the particle flux inevitably decreases the mean particle energy. As a result, the particle loading can be considered as a rather effective mechanism for deceleration of the jet bulk motion as well.

The main goal of this article is to determine more carefully the photon drag action on a cylindrical magnetically dominated outflow. As a zero approximation (i.e. without radiation drag and particle loading), we use the well-known analytical solution for a cylindrical magnetically dominated MHD outflow (Istomin & Pariev 1994; Beskin 2009). As we are interested in the region distant enough from the 'central engine', we consider a simple isotropic model of the radiation field (i.e. energy density $U = U_{\rm iso} = {\rm const}$). Actually, our goal is simply evaluating $U_{\rm iso}$, which is necessary to explain the observable deceleration of jets on a scale of 50–100 pc.

This article is organized as follows. First, in Section 2, the necessity of using a two-fluid MHD approximation for highly magnetized winds and jets in the presence of an external photon field is discussed. In Section 3, starting with the basic two-fluid MHD equations, the appearance of a longitudinal electric field under the drag force redistributing electric charges is established. This makes it possible to determine the change in particle energy. The beam damping resulting from particle loading is discussed in the accompanying article (Beskin & Nokhrina in preparation). Finally, in Section 4 the main results of our study, including astrophysical applications, are formulated.

## 2 A PROBLEM

First, let us formulate the main unsolved problem we are going to discuss. Up to the present, the properties of highly magnetized winds and jets have been mainly described analytically (Michel 1969; Goldreich & Julian 1970; Heyvaerts & Norman 1989; Appl & Camenzind 1992; Beskin, Kuznetsova & Rafikov 1998; Beskin & Nokhrina 2006) and numerically (Komissarov 1994; Ustyugova et al. 1995; Bogovalov & Tsinganos 1999; Komissarov et al. 2007; Tchekhovskoy, McKinney & Narayan 2008, 2009; Bucciantini et al. 2009; Porth et al. 2011; McKinney et al. 2012) using the MHD approximation. Recently, the first steps were made in using the particle-in-cell (PIC) numerical simulation (Sironi & Spitkovsky 2009; Beal, Guillori & Rose 2010), but these explorations are still at the initial stage.

It is important for us to introduce the main dimensionless parameters describing an ideal MHD flow, namely the particle multiplicity $\lambda$, the magnetization parameter $\sigma_{\rm M}$ and the compactness parameter $l_{\rm a}$. First, to describe the flow number density we introduce the so-called particle multiplicity,

$$\lambda = \frac{n^{(\rm lab)}}{n_{\rm GJ}}, \tag{1}$$

where $n_{\rm GJ} = |\rho_{\rm GJ}|/e$ and $\rho_{\rm GJ} = \Omega_0 B_0/(2\pi c)$ is the Goldreich & Julian (1969) charge density, i.e. the minimum charge density required for screening of the longitudinal electric field in the flow. Here $B_0$ is the poloidal magnetic field in a jet and $\Omega_0$ is the central engine angular velocity. As was shown by Nokhrina et al. (2015), for active galactic nuclei the multiplication parameter can be very large: $\lambda \sim 10^{11}$–$10^{13}$.

Next, the Michel (1969) magnetization parameter $\sigma_{\rm M}$ shows by how much the electromagnetic energy flux near the central engine can exceed the particle energy flux. The value $\sigma_{\rm M}$ corresponds to the maximal bulk Lorentz factor of a plasma that can be reached in the case where the entire electromagnetic energy is transferred to the particle flow. In other words, $\sigma_{\rm M}$ is the maximum Lorentz factor that can be achieved in the magnetized wind. For cylindrical flow, $\sigma_{\rm M}$ can be determined as

$$\sigma_{\rm M} = \frac{\Omega_0 e B_0 r_{\rm jet}^2}{4\lambda m_{\rm e} c^3}, \tag{2}$$

where $r_{\rm jet}$ is the jet's transverse dimension.

The usability of these two parameters arises from the fact that their product depends only on the total energy losses $W_{\rm tot}$ and hence can be determined from observations. Indeed, as was shown by Beskin (2010),

$$\lambda\sigma_{\rm M} \sim \left(\frac{W_{\rm tot}}{W_{\rm A}}\right)^{1/2}, \tag{3}$$

where $W_{\rm A} = m_{\rm e}^2 c^5/e^2 \approx 10^{17}$ erg s$^{-1}$. This value corresponds to the minimum energy losses of a 'central engine' that can accelerate particles up to relativistic energies. Hence, we obtain $\lambda\sigma_{\rm M} \sim 10^{14}$ for ordinary jets from active galactic nuclei (AGNs). Another representation of the product $\lambda\sigma_{\rm M}$ is

$$\lambda\sigma_{\rm M} \sim \frac{e E_r r_{\rm jet}}{m_{\rm e} c^2}, \tag{4}$$

where $E_r \sim (\Omega_0 r_{\rm jet}/c) B_0$. As we see, this value corresponds to the total potential drop across the jet.

Finally, the compactness parameter

$$l_{\rm a} = \frac{\sigma_{\rm T} U_{\rm iso} R}{m_{\rm e} c^2} \tag{5}$$

is in fact the optical depth due to Thomson cross-section $\sigma_{\rm T}$ at distance $R$ in a photon field with energy density $U_{\rm iso}$. Below, it is important that the parameter $l_{\rm a}$ provides an upper limit of particle energy in the acceleration region. On the other hand, a large $l_{\rm a}$ is necessary for effective particle production.

It is important to note that we consider only a leptonic model of relativistic jets in this article. For this reason, we normalize all the values on electron mass $m_{\rm e}$. This approach is reasonable for the very central parts of a jet connected with the black hole horizon by magnetic field lines (and hence loaded by secondary $e^+e^-$ plasma generated by photon–photon conversion). The numerical simulations mentioned above demonstrate a regular magnetic field and energy flux in this region. Regarding the peripheral part of a jet connecting with the accreting disc, special consideration including reconnection is necessary. This is beyond the scope of the present approach.

It is important to note that the one-fluid MHD approach has several serious restrictions. Indeed, the well-known freezing-in condition $\boldsymbol{E} + \boldsymbol{v} \times \boldsymbol{B}/c = 0$ results in two consequences:

$$E_{\parallel} = 0, \tag{6}$$

$$E_{\perp} < B, \tag{7}$$

namely a zero longitudinal electric field and a small perpendicular electric field in comparison with the magnetic one. The Ferraro (1937) isorotation law, i.e. the conservation of so-called field angular velocity $\Omega_{\rm F}$ (see below) along magnetic tubes, is the mathematical

Downloaded from http://mnras.oxfordjournals.org/ by guest on October 10, 2016

formulation of this property. As a result, there is a very large potential difference between the centre and the boundary of a jet up to the very end of a flow, where the jet meets the external media (lobes in AGNs, Herbig–Haro (HH) objects in young stellar objects (YSO), stellar wind in close TeV binaries).

On the other hand, it is impossible to describe the interaction of external media with a highly magnetized flow without taking this potential drop into consideration. Indeed, in neglecting $E_\perp$ we fail to take into consideration the role of the Poynting flux, which is the main actor in our play. As a result, during such interactions domains with non-zero longitudinal electric field or with $E > B$ are expected to appear, leading to very effective particle acceleration (Beskin 2010). Nevertheless, for the present the role of the Poynting flux during the interaction with external media has been considered only indirectly, e.g. by adding a large enough toroidal magnetic field, the energy density of which is similar to that of magnetized flow (Bogovalov et al. 2008; de la Cita et al. 2016). Remember that the general properties of a MHD shock containing an arbitrary Poynting flux were formulated more than ten years ago (Double et al. 2004).

Effective particle acceleration can take place even without external media. As was demonstrated many years ago (Beskin, Gurevich & Istomin 1993; Beskin & Rafikov 2000), if there is some restriction on the longitudinal electric current circulating in the magnetosphere of a radio pulsar, the region with $E > B$ appears in the vicinity of the light cylinder $R_{\rm L} = c/\Omega$. As a result, there must be very effective particle acceleration up to the bulk Lorentz factor $\Gamma \sim \sigma_{\rm M}$ in the narrow region $\Delta r \sim R_{\rm L}/\lambda$. It is worth noting that such sudden acceleration was recently proposed to explain pulse TeV radiation from the Crab pulsar (Aharonian, Bogovalov & Khangulian 2012).[1] Moreover, recent PIC modelling of an axisymmetric pulsar magnetosphere (Cerutti et al. 2015) also demonstrates very effective particle acceleration near the light cylinder up to $\gamma \sim \sigma_{\rm M}$.

Here it is important to note that not only the one-fluid but even the two-fluid MHD approximation is insufficient to describe the interaction of a highly magnetized flow with external media. As was shown by Beskin et al. (1993) and Beskin & Rafikov (2000), effective particle acceleration in the domain with $E > B$ is inevitably accompanied by the disappearance of the radial velocity. This implies a many-fluid regime, which cannot be described analytically. The same is true for other dissipative processes, e.g. the magnetic reconnection that was also discussed in connection with energy release in a highly magnetized flow, mainly phenomenologically (Romanova & Lovelace 1992; Drenkhahn & Spruit 2002; Bing & Huirong 2011; McKinney & Uzdensky 2012; Golan & Levinson 2015; Levinson & Globus 2016) and numerically (Takamoto 2013; Barkov & Kommisarov 2016; Del Zanna et al. 2016). In particular, as was shown by Levinson & Globus (2016), in some cases such turbulence can accelerate particles even in the presence of a drag force. These processes are beyond the scope of our present work.

In this article, we are not going to discuss the actual interaction of a jet with external media, but rather try to evaluate the role of the external photon field in the hydrodynamical retardation of a jet. In this case, the two-fluid approximation allows us to consider only a self-consistently longitudinal electric field and disturbance of magnetic surfaces. As a result, a one-fluid validity condition will be formulated.

[1] The title of this article is 'Abrupt acceleration of a cold ultrarelativistic wind from the Crab pulsar'.

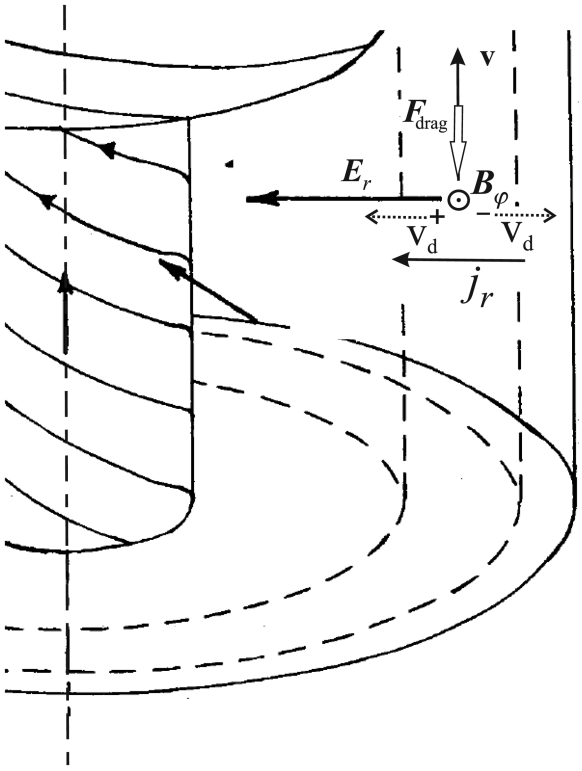


**Figure 1.** Drag force $\boldsymbol{F}_{\rm drag}$ results in the appearance of a radial drift current and redistribution of the electric charges, diminishing the radial electric field and, finally, damping the Poynting flux. The particle energy actually remains constant, as the negative work of the drag force is almost equal to the energy derived from the intersection of equipotential surfaces.

## 3 RADIATION DRAG

### 3.1 Qualitative considerations

First, let us consider the interaction of a magnetically dominated jet with an isotropic photon field from a qualitative viewpoint. Far enough from the axis of rotation, without drag, particle motion along the jet corresponds to an electric drift in radial electric $E_r$ and toroidal magnetic $B_\varphi \gg B_z$ fields (Tchekhovskoy et al. 2008; Beskin 2009). It is clear that the drag force $\boldsymbol{F}_{\rm drag}$ directed along the jet results in the radial drift of electrons and positrons in opposite directions (see Fig. 1). The appropriate electric current can be evaluated as

$$j_r \sim \lambda \rho_{\rm GJ} V_{\rm d}, \tag{8}$$

where

$$V_{\rm d} \sim c \frac{F_{\rm drag}}{e B_\varphi} \tag{9}$$

is the drift velocity. Such the current diminishes the toroidal magnetic field $B_\varphi$. Simultaneously, redistribution of electric charges diminishes the radial electric field $E_r$. These two processes result in a reduction of the Poynting vector flux.

As in the magnetically dominated jet $E_r \approx B_\varphi$, the energy equation for the time-independent flow $\nabla \boldsymbol{S} = -\boldsymbol{j}\boldsymbol{E}$ can be written as

$$\frac{c}{4\pi} \frac{{\rm d}B_\varphi^2}{{\rm d}z} \approx -j_r B_\varphi. \tag{10}$$



Downloaded from http://mnras.oxfordjournals.org/ by guest on October 10, 2016

Using relation (3) and evaluations $B_\varphi/B_z \sim r_{\rm jet}/R_{\rm L}$ and $W_{\rm tot} \sim (c/4\pi)B_\varphi^2 r_{\rm jet}^2$, we finally obtain that the characteristic retardation scale $L_{\rm dr}$:

$$L_{\rm dr} \sim \sigma_{\rm M} \frac{m_{\rm e}c^2}{F_{\rm drag}}. \tag{11}$$

The same evaluation can be inferred directly from the continuity equation $\nabla \boldsymbol{j} = 0$:

$$\frac{j_r}{r_{\rm jet}} \sim \frac{j_\parallel}{L_{\rm dr}}, \tag{12}$$

where $j_\parallel \approx \rho_{\rm GJ} c$.

Hence, the work $A_{\rm dr} = F_{\rm drag} L_{\rm dr}$ done by drag force $F_{\rm drag}$ at distance $L_{\rm dr}$ (resulting in IC photons release of the jet energy flux),

$$A_{\rm dr} \sim \sigma_{\rm M} m_{\rm e} c^2, \tag{13}$$

equals the particle energy corresponding to the total energy transferred from the electromagnetic Poynting flux to the plasma outflow (Beskin & Rafikov 2000). This means that our evaluation of the retardation scale is correct. However, as this force acts almost perpendicular to the large toroidal magnetic field $B_\varphi \sim (\Omega_0 r_{\rm jet}/c)B_0$, the energy of particles remains constant in the first approximation. The point is that the energy loss $-F_{\rm drag} v_z$ resulting from the drag force is fully compensated by the energy $eE_r V_r$ gained by the particles due to their radial drift motion along the radial electric field. In other words, the particle energy actually remains constant, as the negative work of the drag force is almost equal to the energy derived from the intersection of equipotential surfaces.

Thus, the drag force acts on plasma particles in a highly magnetized wind but does not diminish particle energy; only the Poynting-vector flux diminishes as both the toroidal magnetic and radial electric fields decrease along the jet. This was first demonstrated by Beskin et al. (2004). Regarding particle deceleration, this effect arises from the second-order approximation, taking into account the diminishment of integrals of motion.

### 3.2 Cylindrical flow

#### *3.2.1 Basic equations*

In this section, we are going to consider the interaction of a cylindrical magnetically dominated jet with an isotropic photon field quantitatively. Some simplifications are used to analyse this process analytically. First, as has been already stressed, we discuss a leptonic model of relativistic jets. Secondly, we consider below a pure cylindrical jet. This assumption is more serious than one might imagine at the first glance. The point is that cylindrical geometry implies infinite curvature of the poloidal magnetic field. In this case, there is well-known asymptotic behaviour for particle Lorentz factors in the magnetically dominated flow $\Gamma \approx \Omega r_\perp/c$, which will be used in what follows. Remember that, for a finite curvature radius $R_{\rm c}$ of the poloidal magnetic field, another asymptotic solution $\Gamma \approx (R_{\rm c}/r_\perp)^{1/2}$ is possible.

Finally, a magnetically dominated jet (a jet that does not reach its terminal Lorentz factor $\Gamma = \sigma_{\rm M}$) is considered. It is not clear that the flow remains highly magnetized up to distances 10–100 pc from the central engine under this consideration. Nevertheless, this case is more interesting in terms of physics, in that it is able to take into consideration the interaction of the photon field with the Poynting flux. Some astrophysical applications of Fanaroff–Riley Class I and II (FRI–FRII) classification are discussed in Section 4.

Thus, following Beskin et al. (2004), we write down the set of time-independent Maxwell equations and two-fluid equations of motion for an electron–positron plasma:

$$\nabla \boldsymbol{E} = 4\pi\rho_{\rm e}, \qquad \nabla \times \boldsymbol{E} = 0, \tag{14}$$

$$\nabla \boldsymbol{B} = 0, \qquad \nabla \times \boldsymbol{B} = \frac{4\pi}{c}\boldsymbol{j}, \tag{15}$$

$$(\boldsymbol{v}^\pm \nabla)\boldsymbol{p}^\pm = e\left(\boldsymbol{E} + \frac{\boldsymbol{v}^\pm}{c} \times \boldsymbol{B}\right) + \boldsymbol{F}^\pm_{\rm drag}. \tag{16}$$

Here, $\boldsymbol{E}$ and $\boldsymbol{B}$ are the electric and magnetic fields, $\rho_{\rm e}$ and $\boldsymbol{j}$ are the charge and current densities and $\boldsymbol{v}^\pm$ and $\boldsymbol{p}^\pm$ are the speed and momentum of the particles, respectively. Finally, $\boldsymbol{F}_{\rm drag}$ is the radiation drag force. In the case of an isotropic photon field (Blumenthal & Gould 1970; Rybicki & Lightman 1981),

$$\boldsymbol{F}^\pm_{\rm drag} = -\frac{4}{3}\frac{\boldsymbol{v}}{v}\sigma_{\rm T} U_{\rm iso} (\gamma^\pm)^2, \tag{17}$$

where $\gamma^\pm$ are the Lorentz factor of the particles.

As is known, in the axisymmetric case the electric and magnetic fields can be expressed through three scalar functions $\Psi(r_\perp, z)$, $\Omega_{\rm F}(r_\perp, z)$ and $I(r_\perp, z)$:

$$\boldsymbol{B} = \frac{\nabla\Psi \times \boldsymbol{e}_\varphi}{2\pi r_\perp} - \frac{2I(\Psi)}{c r_\perp}\boldsymbol{e}_\varphi, \tag{18}$$

$$\boldsymbol{E} = -\frac{\Omega_{\rm F}(\Psi)}{2\pi c}\nabla\Psi. \tag{19}$$

Here, $\Psi(r_\perp, z)$ is the magnetic flux, $I(\Psi)$ is the total electric current within the same magnetic tube and $\Omega_{\rm F}(\Psi)$ is the so-called field angular velocity (more precisely, the angular velocity of plasma drifting in electromagnetic fields).

There is a force-free solution of the general equations for cylindrical outflow (14)–(16) (Istomin & Pariev 1994):

$$4\pi I(\Psi) = 2\,\Omega_{\rm F}(\Psi)\Psi, \tag{20}$$

corresponding to a homogeneous poloidal magnetic field,

$$B_z^{(0)} = B_0, \tag{21}$$

so that $\Psi^{(0)} = \pi B_0 r_\perp^2$, i.e. it does not depend on coordinate $z$,

$$B_\varphi^{(0)} = -\frac{2I}{c r_\perp}, \tag{22}$$

$$E_r^{(0)} = B_\varphi^{(0)} \tag{23}$$

and

$$B_r^{(0)} = 0, \qquad E_\varphi^{(0)} = 0, \qquad E_z^{(0)} = 0. \tag{24}$$

It is important that this solution can be realized by massless particles only, moving along the jet with a velocity equal to that of light:

$$v_z^{(0)} = c, \qquad v_r^{(0)} = 0, \qquad v_\varphi^{(0)} = 0. \tag{25}$$

Moreover, this solution applies to an arbitrary profile of angular velocity $\Omega_{\rm F}(\Psi)$. In particular, the most interesting case $I(\Psi_{\rm jet}) = \Omega_{\rm F}(\Psi_{\rm jet}) = 0$, corresponding to zero total electric current flowing within the jet, can be considered. For this reason, here and below we consider $\Omega_{\rm F}(r_\perp)$ as an arbitrary function.

As previously discussed, in the cylindrical geometry we seek the first-order corrections for the case $v \neq c$ in the following manner:

$$n^+ = \frac{\Omega_0 B_0}{2\pi c e}\left[\lambda - K(r_\perp) + \eta^+(r_\perp, z)\right], \tag{26}$$



Downloaded from http://mnras.oxfordjournals.org/ by guest on October 10, 2016

$$n^- = \frac{\Omega_0 B_0}{2\pi ce}\left[\lambda + K(r_\perp) + \eta^-(r_\perp, z)\right], \tag{27}$$

$$v_z^\pm = c\left[1 - \xi_z^\pm(r_\perp, z)\right], \tag{28}$$

$$v_r^\pm = c\xi_r^\pm(r_\perp, z), \tag{29}$$

$$v_\varphi^\pm = c\xi_\varphi^\pm(r_\perp, z). \tag{30}$$

Here $\Omega_0 = \Omega_{\rm F}(0)$ and $\lambda = n_{\rm e}/n_{\rm GJ}$ (1) is the multiplicity parameter again. As already stressed, the evaluation $\lambda \sim 10^{11}$–$10^{13}$ is valid for AGNs. Below, in order to simplify, we consider $\lambda$ as a constant. Also,

$$K(r_\perp) = \frac{1}{4r_\perp}\frac{\rm d}{{\rm d}r_\perp}\left(r_\perp^2\frac{\Omega_{\rm F}}{\Omega_0}\right) \tag{31}$$

describes the charge density

$$\rho_{\rm e}^0(r_\perp) = -\frac{\Omega_0 B_0}{\pi c}K(r_\perp) \tag{32}$$

and current density $j_z^0 = \rho_{\rm e}^0 c$ transverse profiles. In particular, $K(0) = 1/2$ and

$$\pi\int_0^{r_{\rm jet}} K(r')r'\,{\rm d}r' = 0, \tag{33}$$

so both the total charge and total longitudinal current in the jet vanish. Finally, the disturbances of the electric potential $\Phi(r_\perp, z)$ and magnetic flux $\Psi(r_\perp, z)$ can be written as

$$\Phi(r_\perp, z) = \frac{B_0}{c}\left[\int_0^{r_\perp}\Omega_{\rm F}(r')r'\,{\rm d}r' + \Omega_0 r_\perp^2\delta(r_\perp, z)\right], \tag{34}$$

$$\Psi(r_\perp, z) = \pi B_0 r_\perp^2\left[1 + f(r_\perp, z)\right]. \tag{35}$$

This gives

$$B_r = -\frac{1}{2}r_\perp B_0\frac{\partial f}{\partial z}, \tag{36}$$

$$B_\varphi = -\frac{\Omega_0 r_\perp}{c}B_0\left[\frac{\Omega_{\rm F}}{\Omega_0} + \zeta(r_\perp, z)\right], \tag{37}$$

$$B_z = B_0\left[1 + \frac{1}{2r_\perp}\frac{\partial}{\partial r_\perp}\left(r_\perp^2 f\right)\right], \tag{38}$$

$$E_r = -\frac{\Omega_0 r_\perp}{c}B_0\left[\frac{\Omega_{\rm F}}{\Omega_0} + \frac{1}{r_\perp}\frac{\partial}{\partial r_\perp}\left(r_\perp^2\delta\right)\right], \tag{39}$$

$$E_z = -\frac{\Omega_0 r_\perp^2}{c}B_0\frac{\partial\delta}{\partial z}. \tag{40}$$

We see that the values $|\delta| \sim 1$ and $|f| \sim 1$ correspond to almost full dissipation of the Poynting flux.

Now, substituting expressions (26)–(40) into (14)–(16), in the first-order approximation we obtain the following linear system of equations:

$$-\frac{1}{r_\perp}\frac{\partial}{\partial r_\perp}(r_\perp^2\zeta) = 2(\eta^+ - \eta^-) - 2\left[(\lambda - K)\xi_z^+ - (\lambda + K)\xi_z^-\right], \tag{41}$$

$$2(\eta^+ - \eta^-) + \frac{1}{r_\perp}\frac{\partial}{\partial r_\perp}\left[r_\perp\frac{\partial}{\partial r_\perp}\left(r_\perp^2\delta\right)\right] + r_\perp^2\frac{\partial^2\delta}{\partial z^2} = 0, \tag{42}$$

$$r_\perp\frac{\partial\zeta}{\partial z} = 2\left[(\lambda - K)\xi_r^+ - (\lambda + K)\xi_r^-\right], \tag{43}$$

$$-r_\perp^2\frac{\partial^2 f}{\partial z^2} - r_\perp\frac{\partial}{\partial r_\perp}\left[\frac{1}{r_\perp}\frac{\partial}{\partial r_\perp}\left(r_\perp^2 f\right)\right] = 4\frac{\Omega_0 r_\perp}{c}\left[(\lambda - K)\xi_\varphi^+ - (\lambda + K)\xi_\varphi^-\right], \tag{44}$$

$$\frac{\partial}{\partial z}\left(\xi_r^+\gamma^+\right) = -\xi_r^+ F_{\rm d}(\gamma^+)^2 + 4\frac{\lambda\sigma_{\rm M}}{r_{\rm jet}^2}\left[-\frac{\partial}{\partial r_\perp}(r_\perp^2\delta) + r_\perp\zeta - r_\perp\frac{\Omega_{\rm F}}{\Omega_0}\xi_z^+ + \frac{c}{\Omega_0}\xi_\varphi^+\right], \tag{45}$$

$$\frac{\partial}{\partial z}\left(\xi_r^-\gamma^-\right) = -\xi_r^- F_{\rm d}(\gamma^-)^2 - 4\frac{\lambda\sigma_{\rm M}}{r_{\rm jet}^2}\left[-\frac{\partial}{\partial r_\perp}\left(r_\perp^2\delta\right) + r_\perp\zeta - r_\perp\frac{\Omega_{\rm F}}{\Omega_0}\xi_z^- + \frac{c}{\Omega_0}\xi_\varphi^-\right], \tag{46}$$

$$\frac{\partial}{\partial z}\left(\gamma^+\right) = -F_{\rm d}(\gamma^+)^2 + 4\frac{\lambda\sigma_{\rm M}}{r_{\rm jet}^2}\left(-r_\perp^2\frac{\partial\delta}{\partial z} - r_\perp\frac{\Omega_{\rm F}}{\Omega_0}\xi_r^+\right), \tag{47}$$

$$\frac{\partial}{\partial z}\left(\gamma^-\right) = -F_{\rm d}(\gamma^-)^2 - 4\frac{\lambda\sigma_{\rm M}}{r_{\rm jet}^2}\left(-r_\perp^2\frac{\partial\delta}{\partial z} - r_\perp\frac{\Omega_{\rm F}}{\Omega_0}\xi_r^-\right), \tag{48}$$

$$\frac{\partial}{\partial z}\left(\xi_\varphi^+\gamma^+\right) = -\xi_\varphi^+ F_{\rm d}(\gamma^+)^2 + 4\frac{\lambda\sigma_{\rm M}}{r_{\rm jet}^2}\left(-\frac{1}{2}\frac{cr_\perp}{\Omega_0}\frac{\partial f}{\partial z} - \frac{c}{\Omega_0}\xi_r^+\right), \tag{49}$$

$$\frac{\partial}{\partial z}\left(\xi_\varphi^-\gamma^-\right) = -\xi_\varphi^- F_{\rm d}(\gamma^-)^2 - 4\frac{\lambda\sigma_{\rm M}}{r_{\rm jet}^2}\left(-\frac{1}{2}\frac{cr_\perp}{\Omega_0}\frac{\partial f}{\partial z} - \frac{c}{\Omega_0}\xi_r^-\right). \tag{50}$$

Here, $\sigma_{\rm M}$ (2) is the Michel magnetization parameter again and $F_{\rm d} \approx l_{\rm a}/R$ is the normalized radiation drag force,

$$F_{\rm d} = \frac{4}{3}\frac{\sigma_{\rm T}U_{\rm iso}}{m_{\rm e}c^2}. \tag{51}$$

### 3.2.2 *Zero MHD approximation*

As already stressed, expression (20) can be considered as a zero force-free approximation describing the cylindrical flow of massless particles. In the absence of a drag force, we can find the exact MHD solution describing a pure cylindrical flow. Indeed, for

$$(\lambda - K)\xi_z^+ = (\lambda + K)\xi_z^- \tag{52}$$

and

$$\xi_\varphi^\pm = x\xi_z^\pm, \tag{53}$$

a cylindrical flow with $\xi_r^\pm = 0$, $\zeta = \delta = f = 0$ results in $\partial/\partial z = 0$. Here and below we use the dimensionless distance from the axis $x_0 = \Omega_0 r_\perp/c$ and

$$x = \Omega_{\rm F}(r_\perp)r_\perp/c. \tag{54}$$



Downloaded from http://mnras.oxfordjournals.org/ by guest on October 10, 2016

We see that in this case it is necessary to introduce a small difference in the velocities of particles,

$$\xi_z^+ - \xi_z^- = \frac{2K}{\lambda}\xi_z \sim \lambda^{-1}\xi_z, \tag{55}$$

where $\xi_z = (\xi_z^+ + \xi_z^-)/2$ is the hydrodynamical velocity. This is unsurprising, because equations (41)–(50) describe the flow in the MHD (not force-free) approximation. On the other hand, the mean particle energy is still a free function.

Below, we use the following notations:

$$\Gamma = \frac{\gamma^+ + \gamma^-}{2}, \quad G = \gamma^+ - \gamma^-, \tag{56}$$

$$P_+ = \frac{\xi_z^+ + \xi_z^-}{2}, \quad P_- = \xi_z^+ - \xi_z^-, \tag{57}$$

$$Q_+ = \frac{\xi_\varphi^+ + \xi_\varphi^-}{2}, \quad Q_- = \xi_\varphi^+ - \xi_\varphi^-. \tag{58}$$

Finally, as a free function we choose

$$\Gamma^2 = \Gamma_0^2 + x^2, \tag{59}$$

where $\Gamma_0 \sim 1$ is the free parameter. Expression (59) corresponds to the well-known analytical asymptotic solution obtained in many articles (see Beskin 2009, and references herein). Then, using relations (52)–(53), one can obtain

$$Q_\pm = xP_\pm, \tag{60}$$

$$P_- = 2\frac{K}{\lambda}P_+, \tag{61}$$

$$Q_- = 2\frac{K}{\lambda}Q_+, \tag{62}$$

$$G = -\Gamma^3(1 - x^2P_+)P_-, \tag{63}$$

where

$$P_+ = \frac{1}{\Gamma(\Gamma + \sqrt{\Gamma^2 - x^2})}. \tag{64}$$

In the last expression, we leave a square root in the denominator to avoid the subtraction of two almost equal values $\Gamma$ and $\sqrt{\Gamma^2 - x^2}$ in the numerator.

### 3.3 Drift approximation

#### *3.3.1 Two-fluid effects*

Now we can use the drag-free MHD solution (52)–(53) and (59)–(64) as a zero approximation and evaluate the action of a drag force, finding small disturbances in the linear approximation. It is clear that in this case all the disturbances including longitudinal electric field $E_\parallel$ are proportional to drag force $F_{\rm drag}$. Thus, under some conditions the electric force $eE_\parallel$ acting on the charged particle can be larger than the retardation drag force $F_{\rm d}$. In this case, one type of particle is accelerated while another is decelerated more efficiently than by action of the drag force alone, resulting in a full stop at some point. Thus, this condition corresponds to the non-hydrodynamical regime. For this reason, determination of the ratio $eE_\parallel/F_{\rm drag}$ is one of the main goals of our study.

Equations (41)–(50) can be simplified in the drift approximation. Indeed, a well-known expression for the drift velocity,

$$\boldsymbol{V}_{\rm dr} = c\frac{(e\boldsymbol{E} + \boldsymbol{F}_{\rm drag}) \times \boldsymbol{B}}{eB^2}, \tag{65}$$

determines two velocity components perpendicular to the magnetic field $\boldsymbol{B}$.

It is necessary to remember that, in the presence of any force $\boldsymbol{F}$ having a longitudinal component to the magnetic field, expression (65) is not valid. On the other hand, in the reference frame in which the force $\boldsymbol{F}$ is parallel to the magnetic field, one finds that

$$\frac{|V_{\rm d}|}{c} = \frac{1 + \epsilon_\perp^2 + \epsilon_\parallel^2 - \sqrt{(1 - \epsilon_\perp^2)^2 + \epsilon_\parallel^2(2 + 2\epsilon_\perp^2 + \epsilon_\parallel^2)}}{2\epsilon_\perp}, \tag{66}$$

where $\epsilon_{\perp,\parallel} = F_{\perp,\parallel}/eB$, the direction of the drift velocity remaining the same. As we see, the difference from the standard expression (65), $|V_{\rm dr}|/c = \epsilon_\perp$, is proportional to $\epsilon_\parallel^2$. Hence, in the linear approximation this correction can be neglected.

As a result, determining all the velocity components and substituting them into equations of motion (47)–(48), as shown in Appendix A, one obtains

$$\frac{\partial\gamma^\pm}{\partial z} = -\frac{(1 - x^2P_+)^2}{(1 + x^2)}F_{\rm d}(\gamma^\pm)^2 \mp \frac{4\lambda\sigma_{\rm M}}{r_{\rm jet}^2}\frac{(1 - x^2P_+)}{(1 + x^2)}\left(-r_\perp^2\frac{\partial\delta}{\partial z} + r_\perp^2\frac{\Omega_{\rm F}}{\Omega_0}\frac{1}{2}\frac{\partial f}{\partial z}\right). \tag{67}$$

Expression (67) (which is one of the main results of our work) can also be obtained directly if we remember that the general expression

$$\frac{{\rm d}\mathcal{E}}{{\rm d}t} = (\boldsymbol{F}_{\rm drag} + e\boldsymbol{E})\boldsymbol{v} \tag{68}$$

in the drift approximation (65) is equal to

$$\frac{{\rm d}\mathcal{E}}{{\rm d}t} = (F_\parallel + eE_\parallel)v_\parallel. \tag{69}$$

In other words, only the longitudinal component of the force (and only the longitudinal component of the velocity) can change the particle energy. This property is responsible for the appearance of the factors $(1 + x^2)^{-1}$ and

$$(1 - x^2P_+) \approx \frac{\Gamma_0}{\Gamma} \ll 1. \tag{70}$$

As we see, together with the drag force (first term) always diminishing the particle energy, equation (67) contains the action of a longitudinal electric field $E_\parallel$ having two sources. In addition to the disturbance of the electric potential $\delta$, longitudinal electric field $E_\parallel$ appears due to a disturbance of magnetic surfaces $f$. The last term obviously vanishes if

$$\delta = \frac{1}{2}\frac{\Omega_{\rm F}}{\Omega_0}f, \tag{71}$$

i.e. if magnetic surfaces are equipotential. Thus, in the self-consistent analysis of the longitudinal electric field, not only the disturbance of electric potential $\delta$ but also the disturbance of the magnetic surfaces $f$ should be included.

As already stressed, all linear disturbances are to be proportional to the drag force $F_{\rm d}$. To determine these relations, let us introduce the values

$$g_+ = \frac{\delta\gamma^+ + \delta\gamma-}{2}, \qquad g_- = \delta\gamma^+ - \delta\gamma-, \tag{72}$$

$$p_+ = \frac{\delta\xi_z^+ + \delta\xi_z^-}{2}, \qquad p_- = \delta\xi_z^+ - \delta\xi_z^-, \tag{73}$$

$$q_+ = \frac{\delta\xi_\varphi^+ + \delta\xi_\varphi^-}{2}, \qquad q_- = \delta\xi_\varphi^+ - \delta\xi_\varphi^-. \tag{74}$$

Downloaded from http://mnras.oxfordjournals.org/ by guest on October 10, 2016

Substituting them into (41)–(50), we obtain

$$q_- = xp_-, \tag{75}$$

$$q_+ = xp_+ + \frac{1}{R_L}\frac{\partial}{\partial r_\perp}(r_\perp^2\delta) - x_0\zeta, \tag{76}$$

$$g_+ = -\Gamma^3 p_+ + x\Gamma^3 P_+ q_+ + \frac{1}{4}x\Gamma^3 P_- q_-, \tag{77}$$

$$g_- = -\Gamma^3(1-x^2P_+)p_- + x\Gamma^3 P_- q_+, \tag{78}$$

$$g_+ = -\frac{(1-x^2P_+)^2}{1+x^2}\Gamma^2(F_{\rm d}z), \tag{79}$$

$$g_- = -\frac{8\lambda\sigma_{\rm M}(1-x^2P_+)}{1+x^2}\frac{r_\perp^2}{r_{\rm jet}^2}\left(\delta - \frac{1}{2}\frac{\Omega_{\rm F}}{\Omega_0}f\right), \tag{80}$$

$$\zeta = -\frac{A}{\sigma_{\rm M}}\Gamma^2(F_{\rm d}z) + 4K\frac{xx_0}{1+x^2}\delta + 2K\frac{1-x^2P_+}{1+x^2}f, \tag{81}$$

$$\frac{1}{r_\perp}\frac{\partial}{\partial r_\perp}\left[r_\perp\frac{\partial}{\partial r_\perp}\left(r_\perp^2\delta\right)\right] + r_\perp^2\frac{\partial^2}{\partial z^2}\delta - \frac{1}{r_\perp}\frac{\partial}{\partial r_\perp}\left(r_\perp^2\zeta\right) = -2\lambda p_- + 4Kp_+, \tag{82}$$

$$-r_\perp^2\frac{\partial^2}{\partial z^2}(f) - r_\perp\frac{\partial}{\partial r_\perp}\left[\frac{1}{r_\perp}\frac{\partial}{\partial r_\perp}\left(r_\perp^2 f\right)\right] = 4\lambda x x_0 p_- - 8x_0\,Kq_+. \tag{83}$$

As is shown in Appendix A, the system of equations (75)–(83) can be rewritten as two second-order ordinary differential equations (A19)–(A20) for $D = x_0^2\delta$ and $F = xx_0 f$, resulting in

$$\frac{{\rm d}^2}{{\rm d}x_0^2}\left(D - \frac{F}{2}\right) - \frac{16\lambda^2\sigma_{\rm M}}{\Gamma^3 x_{\rm jet}^2}\left(D - \frac{F}{2}\right) + \ldots = 0 \tag{84}$$

outside the light cylinder. Hence, the physical branch of equations (A19)–(A20) corresponds to a quickly diminishing solution $(D - F/2) \to 0$ with the spatial scale $\Delta r_\perp \ll r_{\rm jet}$, where

$$\Delta r_\perp = \frac{\Gamma^{3/2}}{4\lambda\sigma_{\rm M}^{1/2}}\,r_{\rm jet}. \tag{85}$$

Thus, for $\Delta r_\perp \ll r_{\rm jet}$ (and for $\lambda\sigma_{\rm M} \gg 1$) one can neglect the left-hand side of equation (80). As we see, in this case we return to the one-fluid MHD condition (71). Finding $q_+$ from (77) and $\zeta$ from (76), we obtain two equations for $p_-$ and $\delta$:

$$2\lambda p_- - \frac{4Kxx_0P_+}{(1-x^2P_+)}\frac{1}{r_\perp}\frac{\partial}{\partial r_\perp}(r_\perp^2\delta) + \frac{16K^2(x^2+1-x^2P_+)x_0^2P_+}{(1+x^2)(1-x^2P_+)}\delta = \frac{4Kxx_0P_+}{(1-x^2P_+)}\frac{A\Gamma^2}{\sigma_{\rm M}}(F_{\rm d}z) - 2\frac{A\Gamma^2}{\sigma}(F_{\rm d}z), \tag{86}$$

$$4\lambda x x_0 p_- - \frac{8\,Kx_0^2}{(1-x^2P_+)}\frac{1}{r_\perp}\frac{\partial}{\partial r_\perp}\left(r_\perp^2\delta\right) + \frac{32K^2x_0^3x}{(1-x^2P_+)(1+x^2)}\delta = \frac{8\,Kx_0x}{(1-x^2P_+)}\frac{A\Gamma^2}{\sigma}(F_{\rm d}z). \tag{87}$$

Here,

$$A(r_\perp) = \frac{r_{\rm jet}^2}{r_\perp^2}\left[1 - \frac{(1-x^2P_+)^2}{1+x^2}\right]\frac{\Omega_0}{\Omega_{\rm F}}, \tag{88}$$

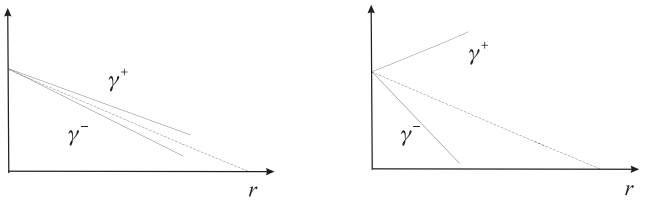


**Figure 2.** Hydrodynamical ($|g_-| \ll |g_+|$) and non-hydrodynamical ($|g_-| > |g_+|$) regimes of drag action. In the first case, Lorentz factors of electrons $\gamma^-$ and positrons $\gamma^+$ actually coincide with the mean value $\Gamma$. In the second case, one type of particle is accelerated while another is decelerated more efficiently than by action of the drag force alone, resulting in a full stop at some point.

so that $x^2A \sim x_{\rm jet}^2 \gg 1$ ($A \sim 1$ for $x \sim x_{\rm jet}$), and we neglect all the terms containing $\partial^2/\partial z^2$ (for small $F_{\rm d}$, derivatives along the jet are small), $x^{-2}$ and $(1 - x^2P_+) \ll 1$. The full version is given in Appendix A.

### 3.3.2 *Qualitative considerations*

First, let us discuss the result obtained above qualitatively; the appropriate numerical evaluations will be given in the next section. Evaluating $r_\perp^{-1}\partial(r_\perp^2\delta)/\partial r_\perp$ as $\delta$, one can obtain

$$\delta = k_\delta\frac{A}{\sigma_{\rm M}}\Gamma^2(F_{\rm d}z), \tag{89}$$

$$p_- = \frac{k_p}{\lambda\sigma_{\rm M}}\frac{KA}{(1-x^2P_+)}\Gamma^2(F_{\rm d}z), \tag{90}$$

where $k_\delta \sim k_p \sim 1$. As we see, together with the clear condition $|\delta| \sim 1$ for the full damping of the Poynting flux, expression (89) for $\delta$ immediately reproduces our evaluation (11) for the length $L_{\rm dr} = \sigma_{\rm M} m_{\rm e}c^2/F_{\rm drag}$; now it can be rewritten as

$$L_{\rm dr} \sim \frac{\sigma_{\rm M}}{\Gamma^2 F_{\rm d}}. \tag{91}$$

Further, using expression (90) for $p_-$, together with (75) and (77), one can obtain

$$g_- \sim \frac{A}{\lambda\sigma_{\rm M}}\,\Gamma^5\,(F_{\rm d}z). \tag{92}$$

Together with (79), this gives

$$\frac{g_-}{g_+} \sim \frac{1}{\lambda\sigma_{\rm M}}\frac{(1+x^2)A}{(1-x^2P_+)^2}\,\Gamma^3. \tag{93}$$

Relation (93) is actually one of our main results, separating hydrodynamical and non-hydrodynamical regimes of drag force action. Indeed, for multiplicity $\lambda > \lambda_\star$ large enough, where

$$\lambda_\star = \frac{x_{\rm jet}^2\Gamma^3}{\sigma_{\rm M}(1-x^2P_+)^2}, \tag{94}$$

the difference in Lorentz factors of electrons and positrons is negligible and we deal with a one-fluid MHD flow. On the other hand, for $|g_-| > |g_+|$ the drag force $F_{\rm drag}$ is smaller than the electrostatic one $eE_\parallel$. As a result, as is shown in Fig. 2, one type of particle is accelerated while another is decelerated more efficiently than by action of the drag force alone, resulting a in full stop at some point. It is clear that in this case a hydrodynamical description is impossible. As condition (94) can be rewritten as

$$\lambda\sigma_{\rm M} = \frac{x_{\rm jet}^2\Gamma^5}{\Gamma_0^2}, \tag{95}$$



Downloaded from http://mnras.oxfordjournals.org/ by guest on October 10, 2016

we see that, according to (3), the non-hydrodynamical regime can be realized for small $W_{\rm tot} < W_\star$, where

$$W_\star = \frac{x_{\rm jet}^4 \Gamma^{10}}{\Gamma_0^4} W_{\rm A}, \tag{96}$$

here again $W_{\rm A} = m_{\rm e}^2 c^5/e^2 \approx 10^{17}$ erg s$^{-1}$. The corresponding Poyting flux is less than

$$S_\star = \frac{x_{\rm jet}^2 \Gamma^{10}}{\Gamma_0^4} W_{\rm A}. \tag{97}$$

Accordingly, in the non-hydrodynamical regime the distance $L_{\rm st}$ to the stop point can be evaluated as

$$L_{\rm st} \sim \frac{\lambda \sigma_{\rm M}}{\Gamma^4 F_{\rm d}}. \tag{98}$$

Finally, in the one-fluid approximation corresponding to condition $|g_-| \ll |g_+|$, we can write

$$\frac{\partial}{\partial z}\Gamma = -\frac{(1 - x^2 P_+)^2}{1 + x^2} F_{\rm d} \Gamma^2. \tag{99}$$

Certainly, it is possible to use this solution for only a small disturbance of the Lorentz factor $\Gamma$. Nevertheless, we can estimate the distance $L_\Gamma$ of the essential diminishing of the bulk particle energy $m_{\rm e}c^2\Gamma$ of the motion on the scale $L$:

$$L_\Gamma \sim \frac{x_{\rm jet}^2 \Gamma}{\Gamma_0^2 F_{\rm d}}. \tag{100}$$

We see that this distance is much larger than $L_{\rm dr}$. This is not surprising, because in the linear approximation, as already stressed, the particle energy actually remains constant. For this reason, it is impossible to use the value $L_\Gamma$ to estimate retardation length.

### 3.3.3 *Quantitative considerations*

Finally, below we present the result of numerical integration of the linear system (86)–(87). Neglecting $p_-$ and the derivatives $\partial/\partial z$, one can obtain the following second-order ordinary differential equation for determination $\delta$ (for more details, see Appendix A):

$$\begin{aligned} &2x \frac{\rm d}{{\rm d}x_0}\left[x_0 \frac{\rm d}{{\rm d}x_0} D\right] - 2x_0 \frac{\rm d}{{\rm d}x_0}\left[\frac{1}{x_0}\frac{\rm d}{{\rm d}x_0}\left(\frac{\Omega_0}{\Omega_{\rm F}} D\right)\right] \\ &\quad + 8x \frac{\rm d}{{\rm d}x_0}\left[K \frac{(x_0 x + \Omega_0/\Omega_{\rm F} - x^2 P_+ \Omega_0/\Omega_{\rm F})}{(1 + x^2)} D\right] \\ &\quad + 8K x_0 \frac{\rm d}{{\rm d}x_0} D - \frac{32 K^2 x_0 (x^2 + 1 - x^2 P_+)}{x(1 + x^2)} D \\ &\quad = -2x \frac{\rm d}{{\rm d}x_0}\left[x_0^2 \mathcal{G}\right] - 8K x_0^2 \mathcal{G}, \end{aligned} \tag{101}$$

where $D = x_0^2 \delta$, $\mathcal{G} = A\Gamma^2 (F_{\rm d} z)/\sigma_{\rm M}$, $x_0 = \Omega_0 r_\perp/c$ and $x = \Omega(r_\perp) r_\perp/c$ again. Regarding the angular velocity profile $\Omega_{\rm F}(r_\perp)$ that determines the coefficient $K$ (31), we use the simplest relation,

$$\Omega_{\rm F}(r_\perp) = \Omega_0 \left(1 - \frac{r_\perp^2}{r_{\rm jet}^2}\right), \tag{102}$$

corresponding to zero total electric charge and electric current within the jet, $\Omega_{\rm F}(r_{\rm jet}) = 0$.

Additional we need to give some clarifications about chosen boundary conditions. As shown in Appendix B, to avoid a longitudinal electric field on the jet axis, it is necessary to put $D(0) = 0$.

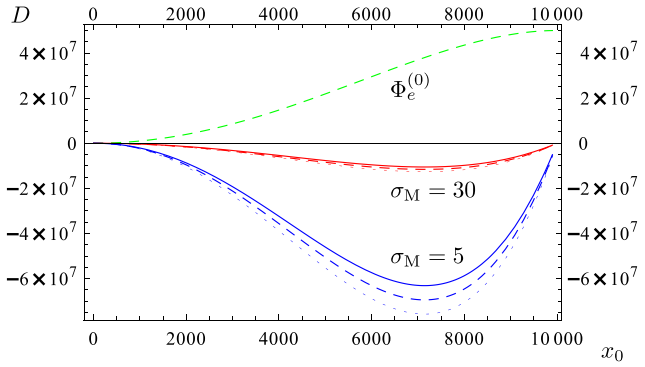


**Figure 3.** Solution $D = x_0^2\delta$ of equation (101) for $x_{\rm jet} = 10^4$ and for different values of $\sigma_{\rm M}$. Solid, dashed and dotted lines for each values of the parameter $\sigma_{\rm M}$ correspond to three different values of $F_d z$: 1, 1.1 and 1.2, respectively. The upper curve corresponds to undisturbed electric potential $\Phi_{\rm e}^{(0)}$.

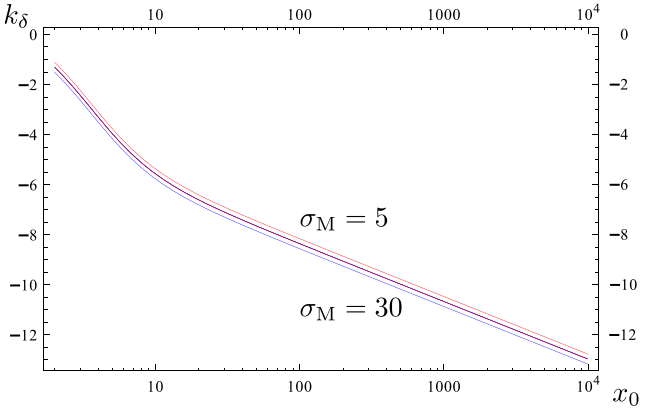


**Figure 4.** Dimensionless function $k_\delta$, which does not actually depend on magnetization parameter $\sigma_{\rm M}$.

Together with the regularity condition at the light cylinder, $x = 1$, this allows us to obtain the full solution of the problem.

As is shown in Fig. 3, the solution of equation (101) gives negative values for the disturbance of electric potential $\delta$. This implies that the disturbance $\delta$ resulting from the drag force compensates gradually for the electric potential of the jet (upper curve). Moreover, as is shown in Fig. 4, our evaluation (89) reproduces the exact solution of equation (101) well enough.

Finally, as, according to (71), the disturbance of magnetic surfaces $f$ should be negative, the magnetic flux $\Psi(r_\perp, z)$ (35) can be rewritten as

$$\Psi(r_\perp, z) = \pi B_0 r_\perp^2 (1 - Cz), \tag{103}$$

where $C > 0$. This leads to the appearance of a positive radial component of the magnetic field $B_r$ (36), i.e. to decollimation of the jet.[2] However, as one can easily check, the width of the jet increases essentially only for $\delta \sim 1$, when almost all electromagnetic energy will be transferred into IC photons.

[2] Here, we consider the case $B_z > 0$.

Downloaded from http://mnras.oxfordjournals.org/ by guest on October 10, 2016

## 4 ASTROPHYSICAL APPLICATIONS AND DISCUSSION

For simple geometry, we have demonstrated the possibility of determining the small correction of the one-fluid ideal outflow resulting from radiation drag force. In comparison with the article by Li et al. (1992), both the disturbance of magnetic surfaces and the electric potential were studied self-consistently. As a result, the method allows us to find the tendency of the drag action on an ideal MHD magnetically dominated outflow, as well as to evaluate the conditions under which this disturbance becomes large.

Let us try to evaluate the real role of radiation drag in the dynamics of relativistic jets in AGNs. The energy density $U_{\rm iso}$ at a distance $R$ from the 'central engine' with total luminosity $L_{\rm tot}$ can be estimated as $U_{\rm tot} \sim 10^{-3}$ erg cm$^{-3}$ at distance $R = 10$ pc. Assuming that $U_{\rm iso} \sim 0.1 U_{\rm tot} \sim 10^{-4}$ erg cm$^{-3}$ (see e.g. Joshi, Marscher & Bottcher 2014), the length of hydrodynamical retardation $L_{\rm dr}$ given by (11) can be estimated as

$$L_{\rm dr} \sim 300 \left(\frac{\sigma_{\rm M}}{10}\right) \left(\frac{\Gamma}{10}\right)^{-2} \left(\frac{L_{\rm tot}}{10^{-4}\,{\rm erg\,cm^{-3}}}\right)^{-1} {\rm pc}. \qquad (104)$$

Thus, for $\Gamma \sim \sigma_{\rm M} \sim 10$, recently obtained by Nokhrina et al. (2015) from analysis of about 100 sources using core-shift technics, the distance is quite reasonable to explain the observable retardation on a scale of $R \sim 100$ pc.

On the other hand, on a scale of $R \sim 10$ kpc, corresponding to the size of the Galaxy, where $U_{\rm iso} \sim 10^{-10}$ erg cm$^{-3}$, the retardation length $L_{\rm dr}$ is too large to prevent the jet material from reaching the lobes. To conclude, in our opinion, an isotropic photon field can be considered as one of the possible reasons for jet deceleration in AGNs.

Finally, it is very interesting to discuss the photon drag action in connection with the Fanaroff & Riley (1974) classification. At first glance, deceleration is more effective in FRII objects, i.e. in objects in which an ambient radiation field is more intense. However, as was demonstrated above, in objects with higher magnetization $\sigma_{\rm M}$ the drag force acts indirectly, diminishing mainly the electromagnetic flux. As far as FRI sources, in which one can expect particle-dominated flow at pc scales, are concerned, drag is much more effective. We are going to consider the statistics of such sources in Paper III.

## ACKNOWLEDGEMENTS

We acknowledge M. Barkov, E. Derishev, Ya. Istomin, M. Drozdova and especially N. Zakamska for useful comments. We also thank the anonymous referee for helpful remarks. This work was supported by the Russian Science Foundation, grant 16-12-10051.

## REFERENCES

Aharonian F. A., Bogovalov S. V., Khangulian D., 2012, Nat, 482, 507
Appl S., Camenzind M., 1992, A&A, 256, 354
Barkov M. V., Komissarov S. S., 2016, MNRAS, 458, 1939
Beal J. H., Guillori J., Rose D. V., 2010, Mem. Soc. Astron. Ital., 81, 404
Begelman M. C., Blandford R. D., Rees M. J., 1984, Rev. Mod. Phys., 56, 255
Beskin V. S., 2009, MHD Flows in Compact Astrophysical Objects. Springer, Berlin
Beskin V. S., 2010, Phys.–Uspekhi, 53, 1199
Beskin V. S., Nokhrina E. E., 2006, MNRAS, 367, 375
Beskin V. S., Rafikov R. R., 2000, MNRAS, 313, 433
Beskin V. S., Gureich A. V., Istomin Ya. N., 1993, Physics of the Pulsar Magnetosphere. Cambridge Univ. Press, Cambridge
Beskin V. S., Kuznetsova I. V., Rafikov R. R., 1998, MNRAS, 299, 341
Beskin V. S., Zakamska N. L., Sol H., 2004, MNRAS, 347, 587
Bing Z., Huirong Ya., 2011, ApJ, 726, 90Z
Blumethal G. R., Gould R. G., 1970, Rev. Mod. Phys., 42, 237
Bogovalov S. V., Tsinganos K., 1999, MNRAS, 305, 211
Bogovalov S. V., Khangulyan D. V., Koldoba A. V., Ustyugova G. V., Aharonian F. A., 2008, MNRAS, 387, 63
Bucciantini N., Quataert E., Metzger B. D., Thompson T. A., Arons J., del Zanna L., 2009, MNRAS, 396, 2038
Cerutti B., Philippov A. A., Parfrey K., Spitkovsky A., 2015, MNRAS, 448, 606
Clausen-Brown E., Savolainen T., Pushkarev A. B., Kovalev Y. Y., Zensus J. A., 2013, A&A, 558, A144
Cohen M. H., Lister M. L., Homan D. C., Kadler M., Kellermann K. I., Kovalev Y. Y., Vermeulen R. C., 2007, ApJ, 658, 232
de la Cita V. M., Bosch-Ramon V., Paredes-Fortuni X., Khangulyan D., Perucho M., 2016, A&A, 591A, 15
Del Zanna L., Papini E., Landi S., Bugli M., Bucciantini N, 2016, MNRAS, 460, 3753
Derishev E. V., Aharonian F. A., Kocharovsky V. V., Kocharovsky Vl. V., 2003, Phys. Rev. D, 68, 043003
Double G. P., Baring M. G., Jones F. C., Ellison D. C., 2004, ApJ, 600, 485
Drenkhahn G., Spruit H. C., 2002, A&A, 391, 1141
Fanaroff B. L., Riley J. M., 1974, MNRAS, 167, 31P
Ferraro V. C. A., 1937, MNRAS, 97, 458
Gabuzda D., Murrey E., Cronin P., 2005, MNRAS, 351, 8
Golan O., Levinson A., 2015, ApJ, 809, 23
Goldreich P., Julian W. H., 1969, ApJ, 157, 869
Goldreich P., Julian W. H., 1970, ApJ, 160, 971
Heyvaerts J., Norman J., 1989, ApJ, 347, 1055
Hirotani K., Okamoto I., 1998, ApJ, 497, 563
Homan D. C., Lister M. L., Kovalev Y. Y., Pushkarev A. B., Savolainen T, Kellermann K. I., Richards J. L., Ros E., 2015, ApJ, 718, 134
Istomin Ya. N., Pariev V. I., 1994, MNRAS, 267, 629
Joshi M., Marscher A. P., Bottcher M., 2014, ApJ, 785, 132
Kardashev N. S. et al., 2014, Phys. Uspehkhi, 57, 1199
Kennel C. F., Fujimura F. S., Okamoto I., 1983, Geophys. Astrophys. Fluid Dyn., 26, 147
Komissarov S., 1994, MNRAS, 269, 394
Komissarov S., Barkov M., Vlahakis N., Königl A., 2007, MNRAS, 380, 51
Lery T., Heyvaerts J., Appl S., Norman C. A., 1998, A&A, 337, 603
Levinson A. Globus N., 2016, MNRAS, 458, 2269
Li Z.-Y., Begelman M., Chiueh T., 1992, ApJ, 384, 567
Lobanov A. P., 1998, A&A, 330, 79
Lyutikov M., 2003, MNRAS, 339, 623
McKinney J. C., Uzdensky D. A., 2012, MNRAS, 419, 573
McKinney J. C., Tchekhovskoy A., Blanford R. D., 2012, MNRAS, 423, 2083
Michel F. C., 1969, ApJ, 158. 727
Nokhrina E. E., Beskin V. S., Kovalev Y. Y., Zheltoukhov A. B., 2015, MNRAS, 447, 2726
Porth O., Fendt Ch., Meliani Z., Vaidya B., 2011, ApJ, 737, 42
Reynolds C. S., DiMatteo T., Fabian A. C., Hwang U., Canizares C., 1996, MNRAS, 283, L111
Romanova M. M., Lovelace R. V. E., 1992, A&A, 262, 26
Russo M., Thompson Ch., 2013a, ApJ, 767, 142
Russo M., Thompson Ch., 2013b, ApJ, 773, 99
Rybicki G. B., Lightman A. P., 1981, Radiative Processes in Astrophysics. John Wiley & Sons, New York
Sikora M., Sol H., Begelman M. C., Madejski G. M., 1996, MNRAS, 280, 781
Sironi L., Spitkovsky A., 2009, ApJ, 698, 1523
Stern B. E., Poutanen J., 2006, MNRAS, 372, 1217
Svensson R., 1984, MNRAS, 209, 175
Takamoto M. 2013, ApJ, 775, 50
Tchekhovskoy A., McKinney J., Narayan R., 2008, MNRAS, 388, 551



Downloaded from http://mnras.oxfordjournals.org/ by guest on October 10, 2016

Tchekhovskoy A., McKinney J., Narayan R., 2009, ApJ, 699, 1789
Thorne K. S., Price R. H., Macdonald D., 1986, Black Holes: The Membrane Paradigm. Yale Univ. Press, New Haven
Ustyugova G. V., Koldoba A. V., Romanova M. M., Chechetkin V. M., Lovelace R. V. E., 1995, ApJ, 439, L39

## APPENDIX A: LINEARIZATION IN THE DRIFT APPROXIMATION

In this Appendix, we determine the linear disturbances to the cylindrical drag-free flow in the drift approximation. First, using the definitions (36)–(38) for a total magnetic field $\boldsymbol{B}$ and clear expressions $\boldsymbol{V}_\parallel = (\boldsymbol{VB})\boldsymbol{B}/\boldsymbol{B}^2$ and $\boldsymbol{V}_\perp = \boldsymbol{V} - \boldsymbol{V}_\parallel$ for any vector $\boldsymbol{V}$, for the perpendicular components of vectors $\boldsymbol{e} = \boldsymbol{E}/B_0$ and $\boldsymbol{F}_{\rm dr}$ we obtain

$$e^r_\perp = -x - x_0 \frac{1}{r_\perp}\frac{\partial}{\partial r_\perp}\left(r_\perp^2\delta\right), \tag{A1}$$

$$e^\varphi_\perp = \frac{x}{(x^2+1)}\left(\frac{1}{2}xr_\perp\frac{\partial f}{\partial z} - x_0 r_\perp\frac{\partial\delta}{\partial z}\right), \tag{A2}$$

$$e^z_\perp = -x_0 r_\perp\frac{\partial\delta}{\partial z} - \frac{1}{x^2+1}\left(\frac{1}{2}xr_\perp\frac{\partial f}{\partial z} - x_0 r_\perp\frac{\partial\delta}{\partial z}\right), \tag{A3}$$

$$F^\varphi_\perp = -\frac{F_{\rm d}\gamma^2}{\sqrt{1-2\xi_z+\xi_\varphi^2}}\frac{(x+\xi_\varphi)}{1+x^2}, \tag{A4}$$

$$F^z_\perp = -\frac{F_{\rm d}\gamma^2 x}{\sqrt{1-2\xi_z+\xi_\varphi^2}}\frac{(x+\xi_\varphi)}{1+x^2}, \tag{A5}$$

$$F^r_\perp = 0. \tag{A6}$$

Using these expressions, we now find for the $r$-component of the drift velocity

$$\xi_r^{\rm dr} = -\frac{(x+\xi_\varphi)}{(x^2+1)}F_{\rm d}\gamma^2 - \frac{xx_0r_\perp}{(x^2+1)}\frac{\partial\delta}{\partial z} \tag{A7}$$

and for the $r$-component of longitudinal velocity

$$(\xi_\parallel)_r = -\frac{1}{2}\frac{(1-x\xi_\varphi)}{(1+x^2)}r_\perp\frac{\partial f}{\partial z}. \tag{A8}$$

Substituting these expressions into (47)–(48) and taking into account that $\xi_\varphi \approx xP_+$ results in (67).

Further, combining (43), (47)–(48) and (67), we find

$$\begin{aligned} r_\perp\frac{\partial\zeta}{\partial z} &= 4Kr_\perp\frac{\Omega_0}{\Omega_{\rm F}}\frac{\partial\delta}{\partial z} \\ &\quad - F_{\rm d}\Gamma^2\left[1-\frac{(1-x^2P_+)^2}{(1+x^2)}\right]\frac{\Omega_0}{\Omega_{\rm F}}\frac{r_{\rm jet}^2}{r_\perp} \\ &\quad + \frac{4K\Omega_0}{r_\perp\Omega_{\rm F}}\frac{(1-x^2P_+)}{(1+x^2)}\left(-r_\perp^2\frac{\partial\delta}{\partial z} + r_\perp^2\frac{\Omega_{\rm F}}{2\Omega_0}\frac{\partial f}{\partial z}\right), \end{aligned} \tag{A9}$$

where we put $(\gamma^+)^2 + (\gamma^-)^2 = 2\Gamma^2$. Integrating, we obtain

$$\zeta = \frac{A}{\sigma}\int F_{\rm d}\Gamma^2\,{\rm d}z + 4K\frac{xx_0}{(x^2+1)}\delta + 2K\frac{(1-x^2P_+)}{(1+x^2)}f, \tag{A10}$$

where $A$ is given by (88). Finally, subtracting equation (46) from (45) and neglecting the left-hand side, we obtain the following expression:

$$q_+ = xp_+ + \frac{1}{R_{\rm L}}\frac{\partial}{\partial r_\perp}\left(r_\perp^2\delta\right) - x_0\zeta, \tag{A11}$$

where again $R_{\rm L} = c/\Omega_0$ is the light-cylinder radius.

Finally, using definitions (56)–(58) and expressing $\gamma^+$ and $\gamma^-$ through $\Gamma$ and $G$, we have

$$\frac{1}{(\Gamma+G/2)^2} = 2\left(P_+ + \frac{P_-}{2}\right) - \left(Q_+ + \frac{Q_-}{2}\right)^2, \tag{A12}$$

$$\frac{1}{(\Gamma-G/2)^2} = 2\left(P_+ - \frac{P_-}{2}\right) - \left(Q_+ - \frac{Q_-}{2}\right)^2. \tag{A13}$$

For $G \ll \Gamma$, this yields

$$G = -\Gamma^3(1-x^2P_+)P_- \tag{A14}$$

and

$$g_- = -(1-x^2P_+)\Gamma^3p_- + xP_-\Gamma^3q_+. \tag{A15}$$

These relations lead to a system of equations (75)–(83).

As a result, expressing $p_+$ from (77) and substituting it together with $\zeta$ in (76), we obtain

$$\begin{aligned} q_+ &= -\frac{x}{\Gamma^3(1-x^2P_+)}g_+ + \frac{1}{(1-x^2P_+)}\frac{1}{R_{\rm L}}\frac{\partial}{\partial r_\perp}(r_\perp^2\delta) \\ &\quad + \frac{x_0}{(1-x^2P_+)}\left[\frac{A}{\sigma}\Gamma^2(F_{\rm d}z) - \frac{4Kxx_0}{(1+x^2)}\delta - \frac{2K(1-x^2P_+)}{(1+x^2)}f\right]. \end{aligned} \tag{A16}$$

Using this in (83), we establish

$$\begin{aligned} &4\lambda xx_0p_- + r_\perp\frac{\partial}{\partial r_\perp}\left[\frac{1}{r_\perp}\frac{\partial}{\partial r_\perp}\left(r_\perp^2f\right)\right] + \frac{16K^2x_0^2}{(1+x^2)}f \\ &+\frac{32K^2x_0^3x}{(1-x^2P_+)(1+x^2)}\delta - \frac{8Kx_0^2}{\left(1-x^2P_+\right)}\frac{1}{r_\perp}\frac{\partial}{\partial r_\perp}\left(r_\perp^2\delta\right) \\ &+r_\perp^2\frac{\partial^2 f}{\partial z^2} = \frac{8Kx_0^2}{(1-x^2P_+)}\frac{A}{\sigma}\mathcal{G} - \frac{8\,Kxx_0(1-x^2P_+)}{1+x^2}\frac{\mathcal{G}}{\Gamma^3}, \end{aligned} \tag{A17}$$

where $\mathcal{G} = \Gamma^2(F_{\rm d}z)$. Additionally, substituting (81) into (82) and expressing $p_+$, we obtain the second equation:

$$\begin{aligned} &2\lambda p_- + \frac{16K^2x_0^2P_+(x^2+1-x^2P_+)}{(1+x^2)(1-x^2P_+)}\delta + r_\perp^2\frac{\partial^2\delta}{\partial z^2} \\ &+\frac{1}{r_\perp}\frac{\partial}{\partial r_\perp}\left[r_\perp\frac{\partial}{\partial r_\perp}(r_\perp^2\delta)\right] - \frac{4}{r_\perp}\frac{\partial}{\partial r_\perp}\left[r_\perp^2\,K\frac{xx_0}{(1+x^2)}\delta\right] \\ &-\frac{2}{r_\perp}\frac{\partial}{\partial r_\perp}\left[r_\perp^2\,K\frac{(1-x^2P_+)}{1+x^2}f\right] \\ &-\frac{4\,Kxx_0P_+}{(1-x^2P_+)}\frac{1}{r_\perp}\frac{\partial}{\partial r_\perp}(r_\perp^2\delta) = -\frac{1}{r_\perp}\frac{\partial}{\partial r_\perp}(r_\perp^2\frac{A}{\sigma}\mathcal{G}) \\ &+\frac{4Kxx_0P_+}{(1-x^2P_+)}\frac{A}{\sigma}\mathcal{G} + \frac{4K(1-x^2P_+)}{\Gamma^3(1+x^2)}\mathcal{G}. \end{aligned} \tag{A18}$$

Neglecting the longitudinal derivatives $\partial^2/\partial z^2$, one can rewrite the system of equations (A17)–(A18) as two second-order ordinary differential equations for $D = x_0^2\delta$ and $F = xx_0f$:

$$\frac{{\rm d}^2D}{{\rm d}x_0^2} = -\frac{1}{x_0}\frac{{\rm d}D}{{\rm d}x_0} + \frac{1}{x_0}\frac{{\rm d}Y}{{\rm d}x_0} - 2\lambda p_- + 4\,Kp_+, \tag{A19}$$



Downloaded from http://mnras.oxfordjournals.org/ by guest on October 10, 2016

$$\frac{\mathrm{d}^2F}{\mathrm{d}x_0^2} = -\left[\frac{1}{x_0} + 2x\frac{\mathrm{d}}{\mathrm{d}x_0}\left(\frac{1}{x}\right)\right]\frac{\mathrm{d}F}{\mathrm{d}x_0} - 4\lambda x^2 p_- + 8Kxq_+ - \left[x\frac{\mathrm{d}^2}{\mathrm{d}x_0^2}\left(\frac{1}{x}\right) + \frac{x}{x_0}\frac{\mathrm{d}}{\mathrm{d}x_0}\left(\frac{1}{x}\right) - \frac{1}{x_0^2}\right]F. \tag{A20}$$

Here, $Y = x_0^2\zeta$,

$$Y = \frac{4Kxx_0}{(1+x^2)}D + \frac{2Kx_0(1-x^2P_+)}{x(1+x^2)}F - \frac{Ax_0^2}{\sigma_\mathrm{M}}\mathcal{G}, \tag{A21}$$

$\mathcal{G} = \Gamma^2(F_\mathrm{d}z)$ and

$$\begin{aligned}
\lambda p_- &= \frac{8\lambda^2\sigma_\mathrm{M}}{\Gamma^3 x_\mathrm{jet}^2(1+x^2)}\left(D - \frac{1}{2}F\right) + \frac{2KP_+x}{(1+x^2)}\frac{\mathcal{G}}{\Gamma^3} \\
&\quad + \frac{2KP_+}{(1-x^2P_+)^2}\frac{\partial}{\partial x_0}D - \frac{2KP_+}{x_0(1-x^2P_+)^2}Y, \\
p_+ &= \frac{(1-x^2P_+)}{(1+x^2)}\frac{\mathcal{G}}{\Gamma^3} + \frac{xP_+}{(1-x^2P_+)}\frac{\partial}{\partial x_0}D - \frac{xP_+Y}{x_0(1-x^2P_+)}, \\
q_+ &= \frac{(1-x^2P_+)x}{\Gamma^3(1+x^2)}\mathcal{G} + \frac{1}{(1-x^2P_+)}\frac{\mathrm{d}D}{\mathrm{d}x_0} - \frac{Y}{x_0(1-x^2P_+)}.
\end{aligned} \tag{A22}$$

Outside the light cylinder, $x_0 \gg 1$, this gives

$$\frac{\mathrm{d}^2}{\mathrm{d}x^2}\left(D - \frac{F}{2}\right) - \frac{16\lambda^2\sigma_\mathrm{M}}{\Gamma^3 x_\mathrm{jet}^2}\left(D - \frac{F}{2}\right) + \ldots = 0. \tag{A23}$$

Hence, the physical branch of equations (A19)–(A20) corresponds to a quickly diminishing solution $(D - F/2) \to 0$ with the spatial scale $\Delta x \ll 1$:

$$(\Delta x)^2 = \frac{\Gamma^3 x_\mathrm{jet}^2}{16\lambda^2\sigma_\mathrm{M}}. \tag{A24}$$

Finally, for $D = F/2$, i.e. in the one-fluid MHD approximation ($E_\parallel = 0$), equations (A17)–(A18) can be restated as (86)–(87). Expressing $p_-$ from (A17) and putting it into (A18), we finally obtain equation (101).

## APPENDIX B: TOY MODEL

A boundary condition $D(0) = 0$ for equation (101) is actually one of the main non-trivial properties of the solution discussed above. The point is that any finite central engine with dipole-like magnetic field produces a quadrupole electric field, so that the potential difference between its magnetic pole and infinity does not vanish. In contrast, our solution corresponds to the zero (more precisely, very small) electric field $E_z$ along the rotational axis.

To demonstrate the possibility for the longitudinal electric field $E_z$ to be small (and vanishing at infinity), let us write down the electric potential in the region $z > 0$ in the form

$$\Phi_\mathrm{e} = \frac{\Omega_0 B_0}{c} r_\mathrm{jet}^2\left(\mathcal{C} + \frac{1}{2}\frac{r_\perp^2}{r_\mathrm{jet}^2} - \frac{1}{4}\frac{r_\perp^4}{r_\mathrm{jet}^4}\right)\exp\left(-\frac{z^2}{L_\mathrm{dr}^2}\right), \tag{B1}$$

where we use expression (102) for angular velocity $\Omega_\mathrm{F}$. For $L_\mathrm{dr} \to \infty$, this corresponds to electric field $E_r^{(0)}$ (23) for arbitrary constant $\mathcal{C}$. In particular, it gives the same zero-order charge density $\rho_\mathrm{e}$ (32). As already stressed, $\mathcal{C} < 0$ ($|\mathcal{C}| \sim 1$) for $L_\mathrm{dr} \to 0$, i.e. for a spatially limited quadrupole charge distribution.

On the other hand, for finite $L_\mathrm{dr}$ the disturbance of charge density in the vicinity of the rotational axis for $z \sim r_\mathrm{jet}$ depends drastically on constant $\mathcal{C}$. Indeed, the additional charge density can be divided into two terms: namely the negative part,

$$\delta\rho_\mathrm{e}^{(1)} = -|\mathcal{C}|\frac{\Omega_0 B_0}{2\pi c}\frac{r_\mathrm{jet}^2}{L_\mathrm{dr}^2}, \tag{B2}$$

existing for $\mathcal{C} \neq 0$ (and producing electric field $E_z < 0$ along the rotation axis opposite the particle flow) and the positive one,

$$\delta\rho_\mathrm{e}^{(2)} = \frac{\Omega_0 B_0}{2\pi c}\frac{z^2}{L_\mathrm{dr}^2}, \tag{B3}$$

having the same order of magnitude on the scale $z \sim r_\mathrm{jet}$. This implies that a small redistribution of the charge density in the base of the flow can indeed screen the longitudinal electric field along the jet.

This paper has been typeset from a TEX/LATEX file prepared by the author.

Downloaded from http://mnras.oxfordjournals.org/ by guest on October 10, 2016